AIAA JOURNAL
Vol. 33, No. 10, October 1995

# Numerical Investigation of Dynamic Stall of an Oscillating Wing

J. A. Ekaterinaris*
*NASA Ames Research Center, Moffett Field, California 94035*

**The unsteady three-dimensional flowfield over an oscillating wing is investigated with the numerical solution of the compressible, time-dependent, Reynolds-averaged Navier–Stokes equations. Spatial discretization is performed with a third-order accurate, upwind-biased, vertex-based, finite volume scheme. An alternative direction implicit, iterative scheme is used for the time integration. The high Reynolds number turbulent flow behavior is modeled with a one-equation turbulence model. The effect of subiterations, time step and grid density on the accuracy of the computed solutions is investigated. It is found that scaling of the time step with the angular velocity of the motion produces accurate solutions at a reduced computational cost. The computational domain over an aspect ratio 5 wing with rounded tip and NACA-0015 airfoil sections is discretized with a single-block grid. The light stall flowfield over the wing oscillating in a subsonic freestream with a mean angle of attack of 11 deg and an amplitude of 4.2 deg is computed. The structure of the separated, unsteady flowfield is investigated and comparisons with available experimental data are performed.**

## Nomenclature

| | |
|---|---|
| $a_\infty$ | = freestream speed of sound |
| $c$ | = chord length |
| $e$ | = total energy |
| $\hat{F}, \hat{G}, \hat{H}$ | = inviscid flux vector |
| $\hat{q}$ | = conservative flow variable vector |
| $\hat{S}$ | = thin-layer approximation of various terms in normal direction |
| $u, v, w$ | = Cartesian velocity components |

## Introduction

THE objective of this investigation is to demonstrate the ability of a recently developed compressible flow solver to simulate the unsteady, three-dimensional unsteady flow effects and generation of dynamic stall over an oscillating wing. The phenomenon of dynamic stall, investigated by McCroskey[1] and McCroskey and Pucci[2] for oscillating airfoils, continues to be a subject of interest in both experimental and theoretical research. An extensive review of experimental and theoretical investigations of dynamic stall is given in Ref. 3. The physical mechanisms involved with dynamic stall are not yet fully understood in spite of their importance to helicopter flight and other aerodynamic applications.

The two-dimensional, low-speed, laminar dynamic stall over airfoils has been the subject of several experimental[4,5] and numerical[6–8] investigations. These investigations provide some insight to the physical mechanisms leading to dynamic stall, but they are not relevant to flowfields of practical interest. For higher freestream speeds, compressibility and turbulent flow behavior play an important role in the generation of dynamic stall and the development of the unsteady flowfield. Recent experimental investigations[9,10] have shown that compressibility effects cannot be ignored for freestream speeds above $M_\infty \approx 0.3$. In Ref. 10 it was also shown that for a freestream speed in the range of $M_\infty \approx 0.4$, multiple shock formation at the leading edge (possibly influenced by the transitional nature of the boundary layer in this region) significantly affects the development of the unsteady flowfield during a pitchup or oscillatory motions. These experimental studies were conducted at Reynolds numbers between 540,000 and 800,000.

Numerical studies[11,12] at the same flow conditions as Ref. 9 have also concluded that transitional/turbulent flow behavior may lead to the development of leading-edge separation bubbles even for steady flows at fixed angles of incidence. Recent numerical investigations[12–15] indicate that leading-edge flow transition may also be of importance for unsteady flows at higher Reynolds numbers of about $4 \times 10^6$. Numerical prediction of low Reynolds number transitional flows, however, involves uncertainties.[11,12] As a result, numerical solutions of such free to transition, unsteady, complex flowfields has had limited success. Fully turbulent unsteady, separated flows are still difficult to predict, but some of the recently developed turbulence models[16–18] show some promise. In this paper the ability of numerical methods to predict three-dimensional dynamic stall in subsonic flow is investigated. To avoid uncertainties associated with the prediction of laminar/transitional/turbulent flows, an experiment where the surface flow has been tripped to ensure fully turbulent boundary layer is simulated.

The two-dimensional dynamic stall over airfoils with fully turbulent, tripped boundary layer has been investigated numerically in Refs. 14 and 19. In Ref. 19 the ability of popular algebraic,[20,21] half-equation,[22] as well as one-equation[16,17] turbulence models in predicting the light and deep stall regimes has been tested. In Ref. 14 one-,[16,17] and two-equation[18,23,24] turbulence models are tested for the same flow conditions. It was found that turbulence models which involve boundary-layer length scales in their formulation are not suitable for the prediction of unsteady flows with large separation. The main reason is that a boundary-layer edge cannot be defined without ambiguity for flows with large separation. A feature of turbulence models that improves their performance and makes them more suitable for the prediction of dynamic stall is their ability to predict separation. It was generally observed[14] that none of the turbulence models could predict accurately the hysteresis effect during the downstroke. In addition, turbulence models which suppress separation, such as the $k-\epsilon$ model, do not predict increase of drag and pitching down moment during the downstroke and lead to premature flow reattachment. Among the models tested in Refs. 14 and 19 the predictions obtained with the Baldwin–Barth[16] (B–B) one-equation turbulence model, even though far from being perfect, were in reasonably good agreement with the experiment. In addition, the ability of this model to predict wing tip vortices for fixed angle-of-attack flows has been tested in Ref. 25, and good agreement with the experiment was obtained. Therefore, in the present investigation the three-dimensional unsteady flowfield is computed with the Baldwin–Barth one-equation turbulence model.

Three-dimensional dynamic stall is of interest in helicopter aircraft and missile aerodynamics. However, few experimental

Received Aug. 5, 1994; presented as Paper 95-0781 at the 33rd Aerospace Sciences Meeting, Reno, NV, Jan. 9–12, 1995; revision received Jan. 23, 1995; accepted for publication Jan. 24, 1995. 

*Research Associate Professor, Navy/NASA Joint Institute of Aeronautics, Naval Postgraduate School, Department of Aeronautics and Astronautics. Member AIAA.

investigations have focused on the three-dimensional flowfield over oscillating and pitching wings. The unsteady, laminar, incompressible flowfield over a pitching wing of aspect ratio 2 has been investigated in Ref. 26. This laminar flow has been simulated numerically in Ref. 27. An extensive experimental investigation of unsteady flowfields over swept and unswept wings for a higher Reynolds number compressible flow has been reported in Refs. 28 and 29. In these investigations the effects of freestream speed and reduced frequency have been also considered. However, the experimental Reynolds number is relatively low and transitional flow behavior reported in Refs. 28 and 29 may introduce additional ambiguities in the application of numerical techniques. In a recent experimental investigation of dynamic stall of an oscillating untwisted wing[30] the boundary layer was tripped at the leading edge. The oscillation amplitude was kept fixed to 4.2 deg and the effects of variation of the mean oscillation angle were investigated. Measurements were obtained for wings with both flat and rounded tip geometries. This experiment provides a good database for testing the ability of numerical methods and turbulence models to predict unsteady turbulent flows and dynamic stall.

In the present investigation numerical solutions for oscillatory motions of the untwisted wing measured in Ref. 30 are obtained. A single-block grid is used for the discretization of the wing with a rounded tip. Essential details of the numerical grid are given in the next section. The upwind-biased numerical scheme used for the solution is described. Convergence tests for unsteady computations and grid refinement studies are presented first. The effects of time step and grid density on the accuracy of the computed solutions are investigated for two-dimensional flow conditions. Comparisons with available experimental data for the three-dimensional flow of the oscillating aspect ratio 5 wing are shown, and the development of the unsteady flowfield is analyzed.

## Numerical Implementation

The thin-layer approximation of the conservative form of the compressible, Reynolds-averaged, Navier–Stokes equations for body-fitted coordinate system $(\xi, \eta, \zeta)$ is used. These equations are as follows:

$$\partial_t \hat{\boldsymbol{q}} + \partial_\xi \hat{\boldsymbol{F}} + \partial_\eta \hat{\boldsymbol{G}} + \partial_\zeta \hat{\boldsymbol{H}} = Re^{-1} \partial_\eta \hat{\boldsymbol{S}} \tag{1}$$

here $\hat{\boldsymbol{q}} = [\rho, \rho u, \rho v, \rho w, e]^T$. In Eqs. (1) all geometrical dimensions are normalized with the wing chord length $c$; the density $\rho$ is normalized with the freestream density $\rho_\infty$; the Cartesian velocity components $(u, v, w)$ of the physical domain are normalized with the freestream speed of sound $a_\infty$; and $e$ is the total energy normalized with $\rho_\infty a_\infty^2$.

The following upwind-biased, factorized, iterative, implicit numerical scheme is used to compute the mean flow:

$$\begin{aligned}
&\left[I + h_\xi\left(\nabla_\xi^b \tilde{A}_{i,j,k}^+ + \Delta_\xi^f \tilde{A}_{i,j,k}^-\right)\right]^p \left[I + h_\eta\left(\nabla_\eta^b \tilde{B}_{i,j,k}^+ + \Delta_\eta^f \tilde{B}_{i,j,k}^-\right)\right]^p \\
&\times \left[I + h_\zeta\left(\nabla_\zeta^b \tilde{C}_{i,j,k}^+ + \Delta_\zeta^f \tilde{C}_{i,j,k}^- - Re^{-1}\delta_\zeta \tilde{M}_{i,j,k}\right)\right]^p \\
&\times \left(\tilde{Q}_{i,j,k}^{p+1} - \tilde{Q}_{i,j,k}^p\right) = -\Big[\left(\tilde{Q}_{i,j,k}^p - \tilde{Q}_{i,j,k}^n\right) \\
&+ h_\xi\left(\hat{F}_{i+\frac{1}{2},j,k}^p - \hat{F}_{i-\frac{1}{2},j,k}^p\right) + h_\eta\left(\hat{G}_{i,j+\frac{1}{2},k}^p - \hat{G}_{i,j-\frac{1}{2},k}^p\right) \\
&+ h_\zeta\left(\hat{H}_{i,j,k+\frac{1}{2}}^p - \hat{H}_{i,j,k-\frac{1}{2}}^p\right) - Re^{-1} h_\zeta\left(\hat{S}_{i,j,k+\frac{1}{2}}^p - \hat{S}_{i,j,k-\frac{1}{2}}^p\right)\Big]
\end{aligned} \tag{2}$$

In this equation, $h_\xi = \Delta\tau/\Delta\xi$, etc. and $\tilde{A}^\pm = (\partial \tilde{F}/\partial \tilde{Q})$, etc. are the flux Jacobean matrices, respectively. The quantities $\hat{F}_{i+1/2,j,k}$, $\hat{G}_{i,j+1/2,k}$, $\hat{H}_{i,j,k+1/2}$, and $\hat{S}_{i,j,k+1/2}$ are inviscid and viscous numerical fluxes, respectively.

The inviscid fluxes $\hat{F}$, $\hat{G}$, and $\hat{H}$ are evaluated using Osher's[31] upwinding scheme. The numerical fluxes for a third-order accurate, vertex-based, upwind-biased scheme are given by

$$\begin{aligned}
\hat{F}_{i+\frac{1}{2},j,k} &= \tilde{F}_{i+\frac{1}{2},j,k} + \frac{1}{6}\left[\Delta F_{i-\frac{1}{2},j,k}^+ + 2\Delta F_{1+\frac{1}{2},j,k}^+\right] \\
&- \frac{1}{6}\left[\Delta F_{i+\frac{3}{2},j,k}^- + 2\Delta F_{1+\frac{1}{2},j,k}^-\right] = \tilde{F}(Q_{i,j,k}, Q_{i+1,j,k}) \\
&+ \frac{1}{6}\left[\Delta F^+(Q_{i+1,j,k}, Q_{i,j,k}) + 2\Delta F^+(Q_{i,j,k}, Q_{i+1,j,k})\right] \\
&- \frac{1}{6}\left[\Delta F^-(Q_{i,j,k}, Q_{i+1,j,k}) + 2\Delta F^-(Q_{i+1,j,k}, Q_{i,j,k})\right]
\end{aligned} \tag{3}$$

here $\tilde{F}$ is the first-order accurate numerical flux for Osher's scheme[31] given by

$$\tilde{F}_{i+\frac{1}{2},j,k} = \frac{1}{2}\left[F_{i,j,k} + F_{i+1,j,k} - \int_{Q_{i,j,k}}^{Q_{i+1,j,k}} \left\{F_q^+ - F_q^-\right\} \mathrm{d}Q\right] \tag{4}$$

where $F_q = F_q^+ + F_q^-$, $F_q^\pm = (\partial F/\partial Q)^\pm$, and $\Delta F^\pm$ are the corrections to obtain high-order accuracy. Two intermediate points are introduced[32] between $i$ and $i+1$ in order to evaluate the integral in Eq. (4). These intermediate points define three subpaths along which the integral is evaluated. Limiting of the high-order discretizations is obtained by modifying the fluxes $\Delta F^\pm$. The gradient of an entropy function $V(Q) = -\rho \log(p/\rho^\gamma)$ is used to switch the order of accuracy at regions of extrema, and the limited fluxes are obtained as it is described in Ref. 32.

For the linearization of the left-hand side terms, the flux Jacobean matrices $A$ and $B$ are evaluated by the Steger–Warming[33] flux-vector splitting. Newton iterations to convergence within each time step are incorporated to reduce linearization and factorization errors and to enhance the time accuracy of the numerical solution. The approximation to $\tilde{Q}^{n+1}$ at each subiteration is the quantity $\tilde{Q}^p$. It will be shown that, typically, two subiterations are sufficient to drop the residuals two orders of magnitude during the Newton iteration process. The viscous fluxes $S_{i,j,k+1/2}$ are computed with central differences. The boundary conditions are specified explicitly. On the wing surface the velocities are set equal to the surface velocity, and the density and pressure are evaluated from the interior by extrapolation. All of the inflow and outflow boundary data are obtained with one-dimensional Riemann invariant extrapolation.

The same numerical scheme was used for the computation of two-dimensional unsteady flows over oscillating airfoils in Refs. 14 and 34. Central difference numerical schemes were used in Refs. 19 and 35 for the computation of two-dimensional unsteady flows over oscillating airfoils. It was found that upwind-biased schemes,[14,34] even though more computationally intensive, provide an advantage for the solution of unsteady flows because they have no dependence on specified numerical dissipation parameters and they appear to have less grid sensitivity compared to central difference schemes.

## Results

Two oscillation cycles are computed for the unsteady solutions. The first cycle, which contains the transients of the restart from a steady solution, is not shown. It was verified that during the second cycle a time-periodic response is obtained and that the third cycle is identical to the second cycle. The accuracy and convergence of the numerical scheme are tested first for two-dimensional flow over an infinite span wing. These solutions are computed first with a baseline $181 \times 5 \times 71$ point C type grid with five identical planes along the spanwise direction. The distance of the first point from the wing surface is 0.00001 chord lengths. Periodic conditions are imposed on the first and last spanwise planes. Grid refinement studies are performed with a $181 \times 5 \times 121$ and a $231 \times 5 \times 121$ point grid. For the first refined grid, only the resolution along the normal direction is increased and the distance of the first point from the wing surface is 0.000005 chord lengths. For the second grid, the suction side streamwise grid resolution is also doubled. Two-dimensional measured data obtained in Ref. 30 for light and deep stall are used to validate computed quasi-three-dimensional solutions for the infinite span wing. The flow is computed at the same freestream speed

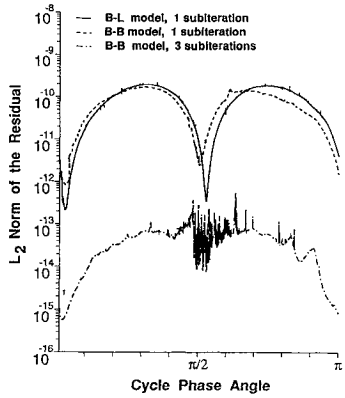


**Fig. 1 Effect of subiterations on convergence, $M_\infty = 0.299$, $\alpha(t) = 11$ deg + 4.2 deg sin($t$), $k = 0.1$, and $Re_c = 1.99 \times 10^6$.**

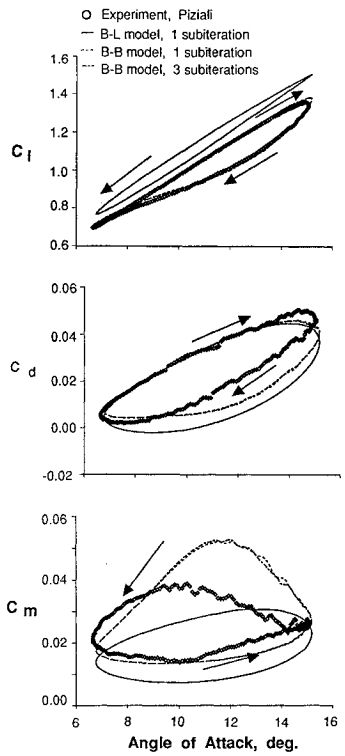


**Fig. 2 Effect of subiterations on the computed loads, $M_\infty = 0.299$, $\alpha(t)$ = 11 deg + 4.2 deg sin($t$), $k = 0.1$, and $Re_c = 1.99 \times 10^6$.**

$M_\infty = 0.299$ and Reynolds number $Re_c = 1.99 \times 10^6$ as the experiment. The boundary layer in the experiment is tripped, and fully turbulent solutions are computed. Only for this two-dimensional flow, in addition to the solutions computed with the one-equation model,[16] a solution with the algebraic Baldwin–Lomax eddy viscosity model[20] is also obtained. Two-dimensional solutions are less computationally intensive and can serve as test case for numerical parameters, such as number of subiterations and time step.

The convergence rates of the $L_{\max}$ norms of the residuals based on density are shown in Fig. 1. In this figure convergence rates achieved with one subiteration and three subiterations for solutions computed with the one-equation model as well as the convergence achieved for the solution computed with the algebraic model and one subiteration are shown. Good convergence is obtained for all computations which are performed with 10,000 time steps per cycle. This number of time steps corresponds to a time step $\Delta t = 0.01$ or a maximum Courant number of about 700. Two to three orders of magnitude higher convergence is obtained when three subiterations are employed. For all cases, during the unsteady solution the residuals show considerable variation in contrast to quasisteady residual variation, but they remain at a low level. The computed lift drag and pitching moment coefficients obtained from these solutions are compared with the experiment in Fig. 2. The solution computed

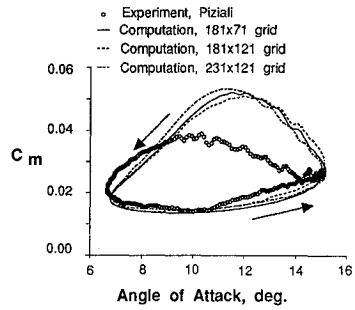


**Fig. 3 Effect of grid refinement on the computed pitching moment, $M_\infty = 0.299$, $\alpha(t) = 11$ deg + 4.2 deg sin($t$), $k = 0.1$, and $Re_c = 1.99 \times 10^6$.**

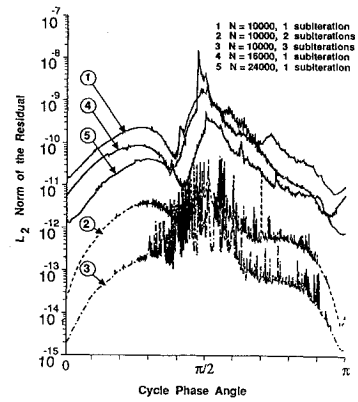


**Fig. 4 Effect of subiterations and time step on convergence, $M_\infty$ = 0.299, $\alpha(t) = 15$ deg + 4.2 deg sin($t$), $k = 0.1$, and $Re_c = 1.99 \times 10^6$.**

with the algebraic model predicts reasonably well the loads during the upstroke. However, it fails to predict separation and yields some discrepancies during the downstroke. It is observed that subiterations do not appear to have a significant effect on the accuracy of the computed loads for this case with limited flow separation.

The effect of grid refinement on the convergence and accuracy of the solution is considered next. Grid refinement is performed first in the normal direction with a 181 × 5 × 121 point grid. A 231 × 5 × 121 point grid with double resolution on the suction side is the finest grid. The refined grid solutions are computed with 10,000 time steps per cycle and one subiteration. The convergence rates achieved on the refined grids (not shown here) are similar to the rate achieved for the baseline grid. The computed lift and drag from both refined grids (not shown here) are in good agreement with the baseline grid predictions. The pitching moment is more sensitive to changes of the surface pressure. The pitching moment hysteresis loops obtained from the solutions with different grid density indicate little grid sensitivity (Fig. 3).

The effect of subiterations and time steps per oscillation cycle on the accuracy of the computed solutions is further investigated for an oscillatory flow around a 15-deg mean angle and 4.2-deg amplitude. For this mean oscillation angle deep stall develops, the unsteady flowfield shows more separation, and nonlinear effects are more pronounced. In Refs. 14 and 19 it was found that a higher grid resolution is required to resolve massive flow separation during the downstroke. For the sake of computational efficiency the baseline grid is used to conduct numerical convergence tests. For this case, only the Baldwin–Barth model is used. The convergence rates achieved for one, two, and three subiterations are shown in Fig. 4. As expected, a significantly higher convergence rate is obtained for more subiterations. In the same figure, the solutions obtained with 16,000 and 24,000 time steps per cycle and one subiteration are shown. A similar convergence rates with the solution obtained with 10,000 time steps per cycle is achieved. Comparisons of the computed loads (Fig. 5) show that the accuracy of the solutions does not improve significantly with subiterations. An increase of time steps per cycle, however, or a reduction of the time step appears to improve the predictions because the measured extreme values of

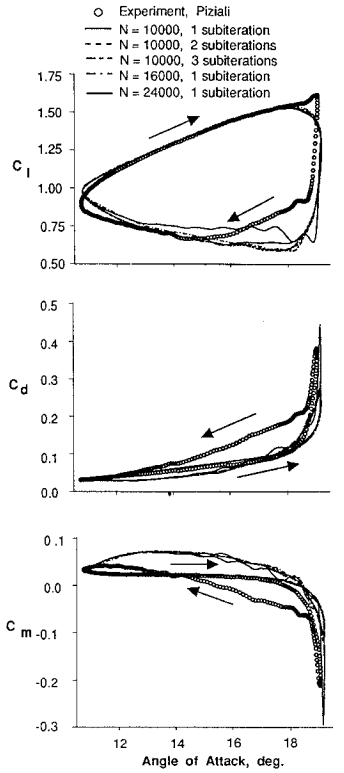


**Fig. 5 Effect of subiterations and time step on the computed loads, $M_\infty = 0.299$, $\alpha(t) = 15$ deg + 4.2 deg sin($t$), $k = 0.1$, and $Re_c = 1.99 \times 10^6$.**

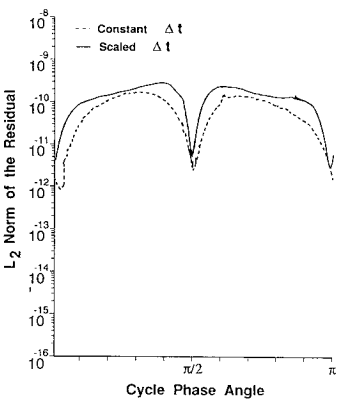


**Fig. 6 Effect of scaled time step on convergence, $M_\infty = 0.299$, $\alpha(t) =$ 11 deg + 4.2 deg sin($t$), $k = 0.1$, and $Re_c = 1.99 \times 10^6$.**

drag and pitching moment are approximated more closely by the solution with 24,000 time steps per cycle. Previous investigations[14] have also suggested that a large unsteady solution for the deep stall case shows small sensitivity at the downstroke.

Numerical solutions with 5000 time steps per cycle have shown that the accuracy of the solution deteriorates even for the light stall case although a converged solution is still obtained. The solution does not improve, however, when 24,000 time steps per cycle are used. On the other hand, the convergence rates obtained with a different number of time steps and one subiteration show that higher convergence is obtained at the low and high incidences during the cycle when the motion is much slower compared to the instant the wing passes through the mean angle of incidence with a high speed. This is an indication that an accurate solution may be still obtained with a higher time step for the parts of the cycle when the motion is slow whereas the time step is low enough when the wing motion is around the mean angle of incidence. The time during the oscillation cycle, therefore, is scaled with the angular velocity as $\tilde{t}(\omega) = t\{1 + \cos[(\omega/\omega_{\max})(\pi/2)]\}$, where $\omega_{\max}$ is the maximum angular velocity obtained at the quarter and three-quarter period of the oscillation. This time scaling yields a large time step for the slow motion during the cycle and smaller time step for the faster parts

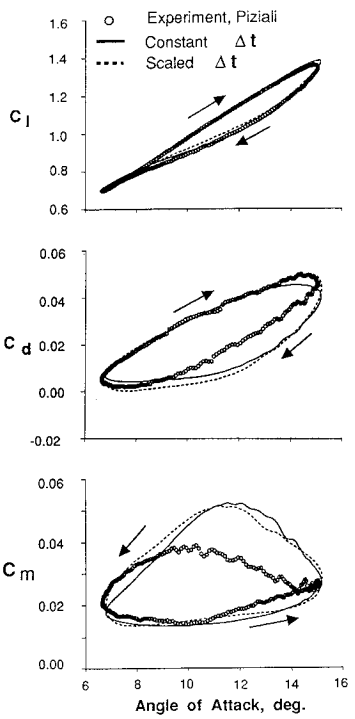


**Fig. 7 Effect scaled time step on the computed loads, $M_\infty = 0.299$, $\alpha(t)$ = 15 deg + 4.2 deg sin($t$), $k = 0.1$, and $Re_c = 1.99 \times 10^6$.**

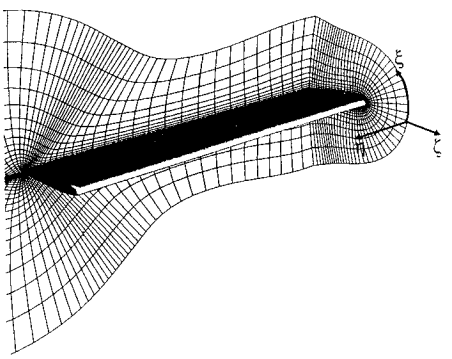


**Fig. 8 Grid over the aspect ratio 5 wing.**

of the cycle. The convergence rate and the computed loads for the oscillatory motion with 4.2-deg amplitude and 11-deg mean-angle where the flow is mildly separated, obtained with a time step scaled with the angular velocity, are compared with the experiment and the solution obtained with 10,000 steps and constant time step in Figs. 6 and 7, respectively. Figure 6 shows that the convergence rate achieved with the scaled time step is more uniform. The computed loads (Fig. 7) are in quite good agreement with the ones obtained with 10,000 iterations and constant time step. When the time step is scaled the cycle is completed with approximately 7000 iterations, which corresponds to savings of 30%.

A single block 181 × 51 × 71 point, C–H type grid along the streamwise $\xi$, spanwise $\eta$, and normal $\zeta$ directions, respectively, is used to discretize the flow domain over the aspect ratio 5 wing. The distance of the first point from the wing surface is 0.00001 chord lengths. Along the streamwise direction 120 points are on the wing and 31 points on each side of the wake. Along the spanwise direction 37 points are on the wing surface. The rounded wing tip is represented with 15 grid lines. The far-field boundaries are approximately 16 chord lengths away from the wing surface. The wing surface and field grid is shown in Fig. 8. At the wing root chord periodic boundary conditions are applied. At the wake cuts at the trailing edge and the wing tip, simple averaging of the flow variables is performed. The inflow and outflow boundary data are obtained by simple one-dimensional Riemann invariant extrapolation.

The numerical tests for the infinite span wing provide confidence for the convergence characteristics and time step and the

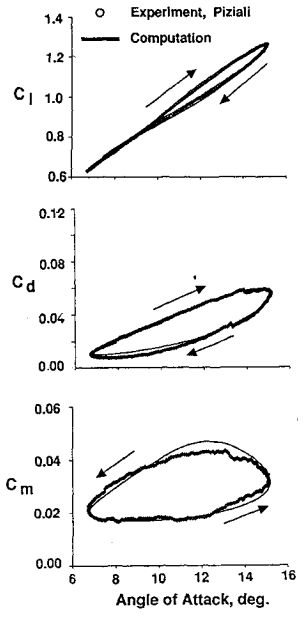


**Fig. 9 Comparison of the computed and measured loads at $y/s = 0.47$, $M_\infty = 0.299$, $\alpha(t) = 11$ deg + 4.2 deg sin($t$), $k = 0.1$, and $Re_C = 1.99 \times 10^6$.**

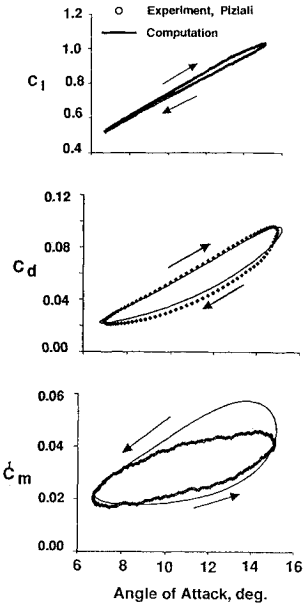


**Fig. 10 Comparison of the computed and measured loads at $y/s = 0.80$, $M_\infty = 0.299$, $\alpha(t) = 11$ deg + 4.2 deg sin($t$), $k = 0.1$, and $Re_C = 1.99 \times 10^6$.**

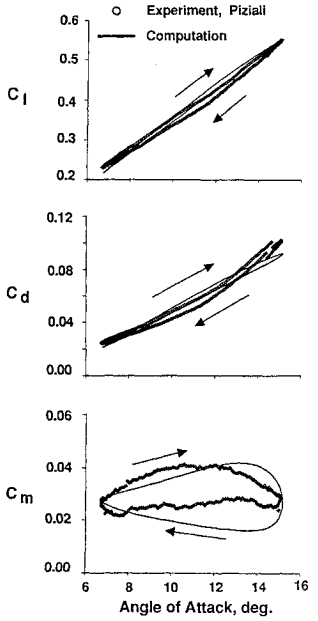


**Fig. 11 Comparison of the computed and measured loads at $y/s = 0.98$, $M_\infty = 0.299$, $\alpha(t) = 11$ deg + 4.2 deg sin($t$), $k = 0.1$, and $Re_C = 1.99 \times 10^6$.**

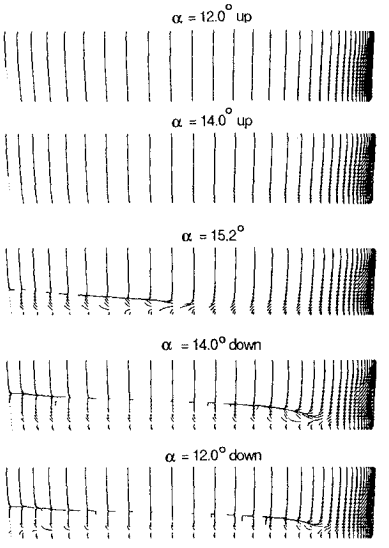


**Fig. 12 Surface flow pattern at $\alpha$ = 12 deg up, $\alpha$ = 14 deg up, $\alpha$ = 15.2 deg, $\alpha$ = 14 deg down, and $\alpha$ = 12 deg down, $M_\infty = 0.299$, $\alpha(t) = 11$ deg + 4.2 deg sin($t$), $k = 0.01$, and $Re_C = 1.99 \times 10^6$.**

grid resolution requirements of the numerical method. The three-dimensional solutions, therefore, are obtained without subiterations. Results for two-dimensional flow test cases have shown that the accuracy of the solution for the deep stall case improves only when 24,000 time steps per cycle are used. The solution over the wing is carried out with 16,000 time steps per cycle because a more severe grid stretching at the tip region results in higher Courant numbers and a time step decrease is required to achieve approximately the same Courant number for the three-dimensional solution as for the two-dimensional test case. The time step is not scaled by the wing angular velocity, but it is kept constant throughout the cycle. Grid refinement has shown little difference in the computed solution for the light stall case. Therefore, for the sake of computational efficiency the baseline 181 × 71 grid resolution is used to represent the two-dimensional wing sections along the span.

The light stall case of Ref. 30, $\alpha(t) = 11$ deg + 4.2 deg sin($t$) is computed for the same flow conditions as in the experiment ($M_\infty = 0.299, k = 0.1$, and $Re_C = 1.99 \times 10^6$). The computed loads at approximately midspan $y/s = 0.47$ are compared with the experiment in Fig. 9. The flow at this location is essentially two dimensional, and the agreement with the experiment is very good. The lift hysteresis (Fig. 9a) is in perfect agreement with the experiment during the upstroke and indicates that a larger flow separation and later reattachment is obtained during the downstroke. This behavior is attributed to the turbulence model and is also observed in Fig. 2 as well as in Refs. 14 and 19 for two-dimensional flows. The computed drag hysteresis (Fig. 9b) is in good agreement with the experiment. The computed pitching moment hysteresis (Fig. 9c) indicates that at the initial part of the downstroke a larger separation is predicted. At midspan it is expected that the flow is essentially two dimensional. Comparison of Fig. 9c with Figs. 2c and 3, however, shows that the three-dimensional measurements at midspan differ from their two-dimensional counterpart.

At the 80% span location where the three-dimensional effects become important, the computed solutions are compared with the available experimental data in Fig. 10. The computed lift hysteresis is in perfect agreement with the experiment throughout the cycle. The numerical solution correctly captures the drop in lift (notice the origin shift of the vertical scale in Fig. 10a) caused by the wing tip downwash also obtained in the experiment. The computed drag and pitching moment hysteresis loops are also in fairly good agreement with the experiment for this location. The unsteady load comparison

at the wing tip $y/s = 0.98$ is shown in Fig. 11. The computation closely follows the experimental trends but fails to show the same quantitative agreement observed at the $y/s = 0.80$ span location. These discrepancies are attributed to inadequate grid resolution at the tip region and the deficiency of the turbulence model to model the wing tip vortex. In Ref. 25 it was shown that even for a steady flow very high grid density and a high-order accurate scheme are needed to accurately capture the tip vortex for a steady flow situation.

The development of the surface flow pattern and the flowfield is shown in Fig. 12 for $\alpha = 12$ deg up, $\alpha = 14$ deg up, $\alpha = 15.2$ deg, $\alpha = 14$ deg down and $\alpha = 12$ deg down. Surface particle traces are used to represent the surface flow. During the upstroke the surface flow remains attached, and flow reversal is obtained at the peak angle of the cycle $\alpha = 15.2$ deg. During the downstroke large flow reversal is observed.

## Conclusions

An upwind-biased iterative flow solver has been developed and utilized to compute unsteady flowfields over oscillating wings. The effects of subiterations, time step, and grid refinement on the convergence rate and the accuracy of the solutions have been investigated. It was found that accurate solutions may be obtained without subiterations and with a reasonable number of time steps per cycle. For mildly separated flows a scaling of the time step with the wing angular speed helped to obtain accurate solutions at a reduced computational cost. The unsteady three-dimensional flowfield over an oscillating aspect ratio 5 wing has been computed. A recently developed one-equation turbulence model was found to be sufficient for capturing the main features of the high Reynolds number turbulent flow behavior.

## Acknowledgment

The support of this investigation by the Naval Air Warfare Center, Weapons Division, China Lake, California, is gratefully acknowledged.

## References

[1]McCroskey, W. J., "The Phenomenon of Dynamic Stall," NASA TM-81264, March 1981.

[2]McCroskey, W. J., and Pucci, S. L., "Viscous Inviscid Interaction on Oscillating Airfoils in Subsonic Flow," *AIAA Journal*, Vol. 20, No. 2, 1982, pp. 167–174.

[3]Carr, L. W., "Progress in Analysis and Prediction of Dynamic Stall," *Journal of Aircraft*," Vol. 25, No. 1, 1988, pp. 6–17.

[4]Walker, J. M., Helin, H. E., and Strikland, J. H., "An Experimental Investigation of an Airfoil Undergoing Large Amplitude Pitching Motions," *AIAA Journal*, Vol. 23, No. 8, 1985, pp. 1141–1142.

[5]Freymuth, P., "Propulsive Vortical Signature of Plunging and Pitching Airfoils," *AIAA Journal*, Vol. 26, No. 6, 1988, pp. 881–883 (AIAA Paper 88-0232).

[6]Metha, U. B., and Zalman, L., "Starting Vortex, Separation Bubbles and Stall: A Numerical Study of Laminar Unsteady Flow Around an Airfoil," *Journal of Fluid Mechanics*, Vol. 67, Pt. 2, 1975, pp. 227–256.

[7]Ghia, K. N., Yang, J., Osswald, G. A., and Ghia, U., "Study of the Role of Unsteady Separation in the Formation of Dynamic Stall Vortex," AIAA Paper 92–0196, Jan. 1992.

[8]Ghosh Choudhuri, P., Knight, D. D., and Visbal, M. R., "Two-Dimensional Unsteady Leading-Edge Separation on a Pitching Airfoil," *AIAA Journal*, Vol. 32, No. 4, 1994, pp. 673–681.

[9]Chandrasekhara, M. S., and Carr, L. W., "Flow Visualization Studies of the Mach Number Effects on Dynamic Stall of an Oscillating Airfoil," *Journal of Aircraft*, Vol. 27, No. 6, 1990, pp. 516–522.

[10]Chandrasekhara, M. S., Ahmed, S., and Carr, L. W., "Schlieren Studies of Compressibility Effects on Dynamic Stall of Transiently Pitching Airfoils," *Journal of Aircraft*, Vol. 30, No. 2, 1993, pp. 213–220.

[11]Ekaterinaris, J. A., Chandrasekhara, M. S., and Platzer, M. F., "Analysis of Low Reynolds Number Airfoils," AIAA Paper 94-0534, Jan. 1994.

[12]Van Dyken, R. D., Ekaterinaris, J. A., Chandrasekhara, M. S., and Platzer, M. F., "Analysis of Transitional Reynolds Number Steady and Oscillatory Airfoil Flows," AIAA Paper 94-2255, June 1994.

[13]Ekaterinaris, J. A., and Platzer, M. F., "Numerical Investigation of Stall Flutter," International Gas Turbine and Aeroengine Congress, American Society of Mechanical Engineers, ASME Paper 94-GT-206, June 1994.

[14]Ekaterinaris, J. A., and Menter, F. R., "Computation of Separated and Unsteady Flows with One and Two-Equation Turbulence Models," AIAA Paper 94-0190, Jan. 1994.

[15]Ekaterinaris, J. A., Srinivasan, G. R., and McCroskey, J. W., "Present Capabilities of Predicting Two-Dimensional Dynamic Stall," 75th Fluid Dynamics AGARD Panel Meeting on Aerodynamics and Aeroacoustics of Rotorcraft, Berlin, Germany, Oct. 1994.

[16]Baldwin, B. S., and Barth, T. J., "A One-Equation Turbulence Transport Model for High Reynolds Number Wall-Bounded Flows," NASA TM 102847, 1990.

[17]Spalart, P. R., and Allmaras, S. R., "A One-Equation Turbulence Model for Aerodynamic Flows," AIAA Paper 92-0439, Jan. 1992.

[18]Menter, F. R., "Zonal Two-equation $k$–$\omega$ Turbulence Models for Aerodynamic Flows," AIAA Paper 93-2906, July 1993.

[19]Srinivasan, G. R., Ekaterinaris, J. A., and McCroskey, W. J., "Dynamic Stall of an Oscillating Wing, Pt 1: Evaluation of Turbulence Models," AIAA Paper 93-3403, Aug. 1993.

[20]Baldwin, B. S., and Lomax, H., "Thin Layer Approximation and Algebraic Model for Separated Turbulent Flows," AIAA Paper 78-257, Jan. 1978.

[21]Yakhot, V., and Orzag, S. A., "Renormalization Group Analysis of Turbulence. 1-Basic Theory," *Journal of Scientific Computing*, Vol. 1, 1986.

[22]Johnson, D. A., and King, L. S., "A Mathematically Simple Turbulence Closure Model for Attached and Separated Turbulent Boundary Layers," *AIAA Journal*, Vol. 23, No. 11, 1985, pp. 1684–1692.

[23]Jones, W. P., and Launder, B. E., "The Calculation of Low-Reynolds-Number-Phenomena with a Two-Equation Model of Turbulence," *International Journal of Heat and Mass Transfer*, Vol. 16, 1973, pp. 1119–1130.

[24]Wilcox, D. C., "Reassessment of the Scale-Determining Equation for Advanced Turbulence Models," *AIAA Journal*, Vol. 26, No. 11, 1988, pp. 1299–1310.

[25]Dacles-Mariani, J., Rogers, S., Kwak, D., Zilliac, G., and Chow, J., "A Computational Study of Wingtip Vortex Flowfield," AIAA Paper 93-3010, Aug. 1993.

[26]Schreck, S. J., and Helin, H. E., "Unsteady Vortex Dynamics and Surface Pressure Topologies on a Pitching Wing," AIAA Paper 93-0435, Jan. 1993.

[27]Newsome, R. W., "Navier–Stokes Simulation of Wing-Tip and Wing-Juncture Interactions for a Pitching Wing," AIAA Paper 94-2259, June 1994.

[28]Lorber, P. F., Covino, A. F., Jr., and Carta, F. O., "Dynamic Stall Experiments on a Swept Three Dimensional Wing in Compressible Flow," AIAA Paper 91-1795, Jan. 1991.

[29]Lorber, P. F., "Compressibility Effects on the Dynamic Stall of a Three-Dimensional Wing," AIAA Paper 92-0191, Jan. 1992.

[30]Piziali, R. A., "An Experimental Investigation of 2D and 3D Oscillating Wing Aerodynamics for a Range of Angle of Attack Including Stall," NASA TM, 1993, to be published.

[31]Osher, S., and Solomon, F., "Upwind Difference Schemes for Hyperbolic Systems of Conservation Laws," *Mathematics of Computation*, Vol. 38, No. 158, 1982, pp. 339–374.

[32]Rai, M. M., and Chakravarthy, S. R., "An Implicit Form of the Osher Upwind Scheme," *AIAA Journal*, Vol. 24, No. 5, 1986, pp. 735–743.

[33]Steger, J. L., and Warming, R. F., "Flux Vector Splitting of the Inviscid Gas Dynamic Equations with Applications to Finite-Difference Methods," *Journal of Computational Physics*, Vol. 40, April 1981, pp. 263–293.

[34]Ekaterinaris, J. A., Cricelli, A. S., and Platzer, M. F., "A Zonal Method for Unsteady, Viscous, Compressible Airfoil Flows," *Journal of Fluids and Structures*, Vol. 8, Jan. 1994, pp. 107–123.

[35]Clarkson, J. D., Ekaterinaris, J. A., and Platzer, M. F., "Computational Investigation of Airfoil Stall Flutter," *Unsteady Aerodynamics, Aeroacoustics and Aeroelasticity of Turbomachines and Propellers*, edited by H.M. Atassi, Springer–Verlag, Berlin, 1991, pp. 415–432.